Open Access

OBM Genetics

Research Article

COMBO-FISH: A Versatile Tool Beyond Standard FISH to Study Chromatin Organization by Fluorescence Light Microscopy

Jin-Ho Lee [1], Florence Laure Djikimi Tchetgna [1], Matthias Krufczik [1], Eberhard Schmitt [1], Christoph Cremer [2], Felix Bestvater [3], Michael Hausmann [1, *]

1. Kirchhoff-Institute for Physics, University of Heidelberg, Im Neuenheimer Feld 227, 69120 Heidelberg, Germany; E-Mails: Jin-Ho.Lee@kip.uni-heidelberg.de, florence@kip.uni-heidelberg.de, matthias@krufczik.de, eschmitt@kip.uni-heidelberg.de, hausmann@kip.uni-heidelberg.de
2. Institute of Molecular Biology, Ackermannweg 4, 55128 Mainz, Germany; E-Mail: c.cremer@imb-mainz.de
3. German Cancer Research Center (DKFZ), Im Neuenheimer Feld 280, 69120 Heidelberg, Germany; Email: f.bestvater@dkfz.de

* **Correspondence:** Michael Hausmann; E-Mail: hausmann@kip.uni-heidelberg.de

Academic Editor: Thomas Liehr

Special Issue: Applications of Fluorescence *in Situ* Hybridization

OBM Genetics
2019, volume 3, issue 1
doi:10.21926/obm.genet.1901064

Received: September 14, 2018
Accepted: January 29, 2019
Published: February 19, 2019

Abstract

***Background*:** Fluorescence In Situ Hybridization (FISH) has become routine for bio-medical research and medical diagnosis, thereby offering a variety of probes and ready-to-use kits that fulfil requirements for many applications. However, conventional FISH relies on chemical and/or thermal denaturation to improve target accessibility and uses huge amounts of DNA that needs to be bonded to the target site. COMBinatorial Oligo-nucleotide FISH (COMBO-FISH) offers possibilities to circumvent these shortcomings.

***Methods*:** COMBO-FISH uses either a set of oligo-nucleotide probes (15 – 25 mers) uniquely co-localizing at the target site or single oligo-stretches repetitively but exclusively binding to the target. These probes are designed by systematic sequence data base searches. COMBO-

FISH probes form Hoogsteen or Watson-Crick bonds, and protocols with or without thermal denaturation can be realized. The latter allows the combination of COMBO-FISH with immunostaining. Low amounts of probe DNA allow the best maintenance of native chromatin organization – a prerequisite for applying super-resolution single molecule localization microscopy (SMLM).

***Results*:** Specific labelling of the *AMACR* gene with an oligo-nucleotide probe set was applied in three different cell types. Hybridization efficiencies were determined by counting spots of high visibility and their radial positions were measured by confocal microscopy. The nuclear architecture revealed a non-random organization. Using uniquely, repetitively binding COMBO-FISH probes for centromere 9, *Alu* consensus and L1 sequences revealed a characteristic probe distribution in cell nuclei as being measured by SMLM. Comparison to theoretical data allowed determination of chromosome 9 radial positions without painting whole chromosomes. Three-color staining by COMBO-FISH for *Alu* and L1 with immunostaining for heterochromatin was successfully demonstrated.

***Conclusions*:** COMBO-FISH is a powerful tool that circumvents shortcomings of standard FISH procedures using probes derived, e.g. from BAC clones. The application for measurements of nuclear architecture by 3D confocal microscopy and of chromatin nano-architecture by SMLM using COMBO-FISH and immunostaining simultaneously has been demonstrated.

Keywords

Fluorescence in situ hybridization; combinatorial oligo-nucleotide FISH (COMBO-FISH); single molecule localization microscopy (SMLM); genome architecture; *AMACR*; *Alu*; centromere 9; L1; heterochromatin

1. Introduction

New insights about three-dimensional organization and architecture of the genome inside the cell nucleus [1-8] have highly impacted recent biological and medical research [9, 10]. In fact, non-random spatial distribution of genomic elements [11-14] in a framework of chromosome territories (CT) and interchromatin compartments (IC) [5-7, 12] has emerged as an additional major regulator of cellular functions and phenotypes [13, 15-19]. Meanwhile, understanding of genome architecture has grown rapidly with the help of modern chromatin conformation capture (3C) derived techniques [20-25] that construct genome-wide maps from formaldehyde crosslinked chromatin interactions. Thereby, mega base-pair sized topologically associating domains (TADs) and subdomains therein (subTADs) [26-29] have been identified as structural units of the three-dimensional genome [30]. In parallel, modern super-resolution microscopy technologies [31-39] have been developed, enabling analyses at the single cell level of cellular nanostructures and molecular interactions on the order of magnitude of single antibodies, histones, receptors, etc. (i.e. in the order of 10 nm) by *in situ* nano-tagging [31]. In this respect, the identification of representative structural parameters as markers for the nano-scale organization of genomic elements in chromatin context is among the central tasks [10, 40, 41]. Therefore, sophisticated methods have emerged from combining labelling with short DNA oligo-nucleotides (< 20

nucleotides) with modern single molecule localization microscopy (SMLM) technologies to localize genomic elements within the nucleus at unprecedented resolution [41].

Fluorescence *in situ* hybridization (FISH) [42] has become a well-established cytometric tool for base-pair complementarity-based labelling of genomic regions using single stranded DNA probes that can be detected via fluorescence microscopy [43]. So far, conventional FISH has been used with great success in biological research and is routinely applied for diagnostics in today's clinics [43]. Nowadays, FISH probes derived from BAC clones are commercially available for many gene targets, all centromeres and telomeres, and for painting of whole chromosomes or large parts of chromosomes. In most cases, ready-to-use kits are the tools of choice. However, in cases of i) gene targets where such kits are not commercially available, ii) non-model species like gorilla or chimpanzee that are completely sequenced nowadays or especially iii) studies on the genomes of plants, oligo-based FISH techniques have become powerful new tools for chromosome identification and karyotyping research [44]. In addition, conventional FISH preparation protocols, as often being established, require harsh thermal (70 °C or more) and chemical denaturing conditions [45, 46] using chaotropic agents like formamide. Under such conditions, the native chromosomal and chromatin structures may be altered [47], especially on the nano- or even on the meso-scale.

Target sequence and length of conventionally used FISH probes derived from yeast artificial chromosomes (YAC) or bacterial artificial chromosomes (BAC) are limited by their design and amplification methods, for instance, the amplified DNA sequences rely on the presence of cuttable sites for restriction enzymes. Due to the patent situation, companies have constructed different probes for the same target that only partly cover the target or only bind to the close neighborhood of a given target. For many purposes in research using conventional light microscopy, this may be sufficient and lead to a tolerable error, since the deviation of exact target labelling is less or similar to the resolution limit.

With the completion of the human reference genome [48] and the establishment of automated oligo-nucleotide synthesis, the basis for design and realization of short oligo-nucleotide probes has been laid. Exact sequence and length of these probes can be computationally optimized to specifically bind to any genomic target. Due to the short size of oligo-probes, which could be selected according to a consistent melting temperature range, these probes are able to cross cell barriers and bind to their intended target. New companies offer free assistance in designing probes, which have been successfully used in specialized applications and in a variety of cell types. Libraries containing hundreds of thousands of such short oligo-nucleotide probes, also termed oligopaint probes, can be used to label genomic regions in the range of kilo- and mega-bases [49-52] with a considerable high signal/noise ratio.

An alternative oligo-nucleotide approach is combinatorial oligo fluorescence *in situ* hybridization (COMBO-FISH) that uses either a unique oligo-probe, of which multiple stretches are binding specifically to a target, or a combinatorial set of a few (about 15 – 25 nt) short DNA probes that are designed to co-localize only at the desired genomic target [53]. This latter approach ensures and enhances labelling specificity even when individual short oligo-nucleotide probes are less unique by statistical nature. Furthermore, the number of binding oligo-nucleotides can be well estimated for a given target so that super-resolution microscopy may allow structural interpretations of chromatin targets [54].

COMBO-FISH can be further extended to triplex forming oligo-nucleotides (TFOs) that directly bind into the major groove of the target sequence via Hoogsteen base-pairing [55-57] and probes consisting of peptide nucleic acids (PNAs) can be also used instead [53, 55, 57, 58]. As no denaturing of the target double-strand is required for TFO probes, labelling of genomic targets can be obtained at maximal conservation of the three-dimensional structure of native chromatin, thereby using only some ten oligo-probes, which result in a few hundred bases of additional DNA only. COMBO-FISH probes are *in silico* designed [55] [59] either with data from open accessible sequence databases, e.g. NCBI [60] or from user-made databases, which could be customized only for TFO-binding sites. These improvements make oligo-nucleotide-based FISH labelling a suitable approach for genome architecture research. Compared to the oligopaint approaches described above, special care must be taken in specimen preparation in order to avoid background signals since the COMBO-FISH label using some ten oligo-nucleotides is often weak. For instance, a set of 20 oligo-nucleotide probes, each one labelled with one dye molecule at the 5' end, forms a fluorescent signal on a gene target that consists of not more than 20 fluorochromes (or maximum 40 fluorochromes, if the 3´end is additionally tagged). In case some oligo-nucleotides have additional binding sites outside the given target or if specimens could not be prepared without un-specific fluorescence, one may run into the trouble of a poor signal/noise ratio. Thus, each FISH approach has its strength and weakness and should be selected according to the requirements of the scientific investigation it is applied to.

COMBO-FISH probe sets, either using triplex-forming, i.e. Hoogsteen binding or double-strand forming, such as Watson-Crick binding probes, were successfully applied in various studies for a variety of genomic regions (e.g. centromere 9 [56], receptor tyrosine kinase 2 (HER2/NEU) [61], breakpoint cluster region (BCR) [62, 63], ABL proto-oncogene 1 (ABL) [62-64], and genomic *Alu* elements [31, 65]). Oligo-nucleotide labelling localization microscopy [39, 66, 67] of *Alu* elements revealed structural changes in chromatin after irradiation [65] and was discovered as a novel dosimetric marker for low [31] to high [65] dose ranges. Results from nanoscopy of COMBO-FISH labelled trinucleotide expansions in the *FMR1* gene promoter represent microscopic counting of repetitive units, which could be addressed as first steps towards realization of *in situ* optical sequencing [54].

In parallel to improvements of COMBO-FISH, sophisticated super-resolution fluorescence microscopy has been developed (e.g. photoactivated localization microscopy (PALM) [33], fluorescence PALM (F)PALM [34], stochastic optical reconstruction microscopy (STORM) [35, 68], direct stochastic optical reconstruction microscopy (dSTORM) [36], ground state depletion microscopy followed by individual molecule return (GSDIM) [37], super-resolution optical fluctuation imaging (SOFI) [38], etc.), which allows nanometer precise localization of fluorescently labelled biomolecules at the single cell level. Spectral position determination microscopy (SPDM) [39] or single molecule localization microscopy (SMLM) uses reversible photo-bleaching at high power laser (kW/cm^2) excitation [69]. Thereby, stochastic recovery of sparse subpopulations of fluorophores from reversible dark states back to fluorescing states (= 'blinking') results in optical isolation through time. This allows precise position determination far below the diffraction limit down to the 10-nm level. SMLM gets full benefit from COMBO-FISH as resolution of labelling and resolution of signal detection lie in matching regimes [54, 56].

In this study, we present results on the application of COMBO-FISH for spatial analysis of the alpha-methylacyl-CoA racemase (*AMACR*) gene locus (P504S) relative to the cell nucleus. This gene

locus is a typical example where most commercially available ready-to-use BAC probes do not individually map the target but overlap over a certain chromosome region on chromosome 5. Therefore, a specific combination of oligo-nucleotides can be used as an alternative for a focused labelling of the given target side only.

The *AMACR* gene codes for an enzyme involved in peroxisomal beta oxidation of branched fatty acids [70, 71] and is highly overexpressed in prostate cancer [72, 73], the most prevalent cancer in the male population, and is used as a well-established diagnostic marker. However, the exact mechanisms causing dysregulation of *AMACR* expression remain elusive [74, 75]. Besides epigenetic impact on dysregulation of genes in tumor genesis significant spatial re-arrangements of the genes or even the gene carrying chromosomes have been shown (see for instance [76]). Spatial analyses of the *AMACR* gene locus in connection with genome architecture can therefore be seen as a new alternative step to gain further insights into the mechanisms of gene regulation and prostate cancer genesis. Here, we show that this focused labelling of a gene target leading to a small fluorescent spot in the cell nuclei can be used as typical examples where an exact positioning of the probes to the target side is required for fluorescence microscopy.

Furthermore, we extend COMBO-FISH by dual color labelling to study the spatial distribution of genomic *Alu* elements around chromosome 9 centromeres. In order to study higher order chromatin networks, low denaturing conditions and SMLM were applied. The uniquely binding short probes better maintain the native structure and resolve the chromatin arrangements in a pointillist manner with a resolution in the 10-nm range. This will allow us to estimate not only the chromosome territory around the centromere but also slight differences in chromatin compaction and sizes between the homologous territories. Moreover, the low temperature conditions allow the simultaneous combination of COMBO-FISH and immunostaining, as demonstrated by the application of Alu- and L1-oligo-probes in combination with H3K9me3 antibody labelling. By this first methodological approach, we will demonstrate new perspectives for investigations of 3D chromatin architecture on the nano-scale with functional relevance.

2. Materials and Methods

2.1 Cell Culture

2.1.1 Human Blood Lymphocytes

Peripheral blood mononuclear cells (PBMCs) were isolated from the blood of a healthy male adult donor by standard density gradient centrifugation (FicoLite H; Linaris, Bettingen a.M., Germany). Interface cells were collected, washed in RPMI 1640 with L-glutamine supplemented with 50% fetal calf serum (FCS; both from PAA Laboratories GmbH, Pasching) and cultivated in chromosome medium B with phytohemagglutinin (PHA; Biochrom KG, Berlin) for no more than 72 hours (approximately, 5 cell divisions) at 37 °C, 5% CO_2 and H_2O saturation. Lymphocytes were seeded on poly-L-lysine hydrobromide (1 mg / mL; Sigma-Aldrich Chemie GmbH, Buch CH) coated microscopy slides for 10 to 60 min to appropriate attachment and fixed in 4% formaldehyde (Fluka Biochemica GmbH, Buchs CH) in 0.3 x PBS for 10 min at room temperature.

2.1.2 VH7 & LNCAP

Human foreskin fibroblast VH7 cells were kindly provided by Prof. Boukamp (Division of Genetics of Skin Carcinogenesis, German Cancer Research Center (DKFZ), Heidelberg). VH7 cells were cultivated in DMEM (Invitrogen GmbH, Karlsruhe) supplemented with 1% penicillin / streptomycin and 10% FCS (all from PAA Laboratories GmbH, Pasching). Human prostate cancer LNCAP cells were cultivated in RPMI 1640 with L-glutamine supplemented with 1% penicillin / streptomycin and 10% FCS (all from PAA Laboratories GmbH, Pasching). All cells were incubated at 37 °C, 5% CO2 and H2O saturation. For specimen preparation, cultivated cells were trypsinized and diluted down to a concentration of 150,000 cells per mL. 1 mL cell suspension was seeded per cover glass within 6-well plates and grown 1 to 2 days to appropriate confluency. Then, cells were washed once in 1 x PBS (Sigma-Aldrich Chemie GmbH, Steinheim) and fixed in 4% formaldehyde (in 1 x PBS; Fluka Biochemica GmbH, Buchs CH) for 10 min at room temperature and washed again in 1 x PBS.

2.1.3 SkBr3 (also known as SK-BR-3)

Human breast cancer SkBr3 cells (ATCC HTB-30) were cultivated in McCoy's 5A (Modified) Medium, GlutaMAX supplemented with 1% penicillin / streptomycin (all Thermofisher, Waltham, MA, USA), 10% FCS (Biochrom, Berlin, Germany), and 25 mM 2-(4-(2-Hydroxyethyl)-1-piperazinyl)-ethan sulfonic acid (HEPES) (Carl Roth, Karlsruhe, Germany) was used. Cells were incubated at 37 °C, 5% CO_2 and H_2O saturation. For specimen preparation, SkBr3 cells were seeded on 24 mm x 24 mm cover glasses (thickness class 1; Wenzel Gläser, Berlin, Germany), in six-well plates (Greiner Bio-One International, Frickenhausen, Germany) and grown to 70% confluency. Cells were washed once with 1 x PBS prior to fixation in 3.7% formaldehyde (in 1 x PBS) for 10 min at 37 °C and washed three times in 1 x PBS + Mg/Ca for 5 min.

2.2 COMBO-FISH Labelling of AMACR Gene Locus in Human Blood Lymphocytes

Formaldehyde (freshly prepared from paraformaldehyde) fixed human blood lymphocytes were treated with RNase (10 mg / mL in Tris-HCl; pH 7.5 + 15 mM NaCl; Sigma-Aldrich Chemie GmbH, Steinheim) at 37 °C for 1 hour and pepsin (100 mg / ml; Sigma-Aldrich Chemie GmbH, Steinheim) at 37 °C for 1 to 3 min depending on the cytoplasmic content of cells. Cells were dehydrated in an increasing ethanol series (70%, 90%, 100%) for 3 min at each concentration. Denaturation was performed in 70% formamide (in 2 x SSC, pH7; Sigma-Aldrich Chemie GmbH, Steinheim) at 75 °C for 5 min and then dehydrated in an increasing ethanol series (70%, 90%, 100%). 100 pmol / µL oligo probes in hybridization buffer (50 mM $MgCl_2$ x 6 H_2O; J.T. Baker B.V., Devender NL) + 3 M NaCl + 0.5 M sodium acetate at pH 7.0) were applied directly onto the cells, immediately covered with a cover glass, and sealed with rubber cement (Fixogum). Hybridization of the probe set (Table 1) was performed in a humidified environment in darkness at 37 °C overnight. Post-hybridization washing was performed in 2 x SSC at 65 °C for 5 min. Cells were counterstained with TOPRO-3-iodide and embedded in Vectashield mounting medium and sealed with Fixogum or nail polish (for long-term preparations).

2.3 COMBO-FISH Labelling of Genomic Alu and Chromosome 9 Centromere in SkBr3 Cells

Formaldehyde fixed SkBr3 cells on cover glasses were permeabilized in 0.1% Triton-X (in 1 x PBS + Mg/Ca) for 3 min. After washing three times in 1 x PBS + Mg/Ca on a shaker for 5 min, cells were incubated in 0.1 M HCl for 10 min, then washed again three times in 1 x PBS + Mg/Ca on a shaker for 5 min. Cell were equilibrated in 2 x SSC for 5 min and denatured in 50% formamide in 2 x SSC at 70 °C for 30 min. 200 ng oligo probes specific for genomic *Alu* (Alexa Fluor® 568-TAATCCCAGCACTTTGG) and 200 ng oligo probes against chromosome 9 centromere (Alexa Fluor® 488-AATCAACCCGAGTGCAAT*)* mixed in 20 µL 10 mM Tris-HCl were pipetted on a clean microscope slide and cover glasses were applied with cells facing down to droplet. Cover glasses were sealed with rubber cement (Fixogum) to prevent drying out and incubated in a humidified environment at 37 °C for 24 hours. Post-hybridization washing was performed in 2 x SSC at 37 °C for 5 min. After equilibrating in 1 x PBS + Mg/Ca for 5 min, cells were counterstained with DAPI and embedded in ProLong Gold Antifade Mountant (ThermoFisher Scientific, Darmstadt, Germany). After curing for 24 hours, specimen were sealed in nail polish and stored at 4 °C in darkness.

2.4 Combined COMBO-FISH and Antibody Labelling of Genomic Alu, L1 and H3K9me3 Heterochromatin in SkBr3 Cells

Three-color staining of H3K9me3, genomic *Alu* and L1 was optimized and performed based on a protocol for low temperature combinatorial oligo-nucleotide FISH (COMBO-FISH) in combination with immunostaining that was previously developed in our group [65].

In brief, formaldehyde fixed SkBr3 cells on cover glasses were permeabilized in 0.1% Triton-X (in 1 x PBS + Mg/Ca) for 3 min. After washing three times in 1 x PBS + Mg/Ca on a shaker for 5 min, cells were blocked in 2% bovine serum albumin (BSA; in 1 x PBS + Mg/Ca) for 30 min. Anti-H3K9me3 rabbit primary antibodies were applied, and cells were incubated in a humidified environment at 37 °C for 30 min. After washing three times in 1 x PBS + Mg/Ca on a shaker for 5 min, cells were incubated with anti-rabbit Alexa Fluor® 647 labelled secondary antibodies at 37 °C for 30 min. After washing three times in 1 x PBS + Mg/Ca on a shaker for 5 min, post fixation was performed in 2% formaldehyde solution (in 1 x PBS + Mg/Ca) at 37 °C for 10 min.

After washing, cells were incubated in 0.1 M HCl for 10 min, then wash-permeabilized three times in 0.05% Triton-X (in 1 x PBS + Mg/Ca) on a shaker for 5 min, equilibrated in 2 x SSC for 5 min, and denatured in 50% formamide in 2 x SSC at room temperature for 30 min. 200 ng oligo probes specific for genomic *Alu* (Alexa Fluor® 568-TAATCCCAGCACTTTGG) and 200 ng oligo probes specific for genomic L1 (Alexa Fluor® 488-*GGTGATTTCTGCATTTC)* mixed in 20 µL 10 mM Tris-HCl were pipetted on a clean microscope slide, and cover glasses were applied with cells facing down to droplet. To prevent drying during hybridization, cover glasses were sealed with rubber cement (Fixogum) and incubated in a humidified environment at 37 °C for 24 hours. Post-hybridization washing was performed in 2 x SSC at 37 °C for 5 min. After equilibrating in 1 x PBS + Mg/Ca for 5 min, cells were counterstained with DAPI and embedded in ProLong Gold Antifade Mountant (ThermoFisher Scientific, Darmstadt, Germany). After curing for 24 hours, specimen can be sealed in nail polish and stored at 4 °C in darkness.

In contrast to the specimens using for CLSM, which were embedded in Vectashield, the specimens for SMLM were embedded in ProLong Gold. In accordance with all projects running on

SMLM in our group, well polymerized ProLong Gold embedding does not influence the blinking efficiency of the dye molecules or show any self-blinking effects.

2.5 Microscopy

2.5.1 Confocal Laser Scanning Microscopy

Fluorescence microscopy was performed on a confocal laser scanning microscope (CLSM) TCS NT-type (Leica) with a PL APO 63 x 1.4 objective (oil immersion) using appropriate filter settings for the dyes used. Images were acquired with a voxel size of 77 nm x 77 nm x 203 nm, zoom factor 4, accumulation factor 4 and saved. Raw images were pre-processed by thresholding in ImageJ prior to further image analysis. 2D maximum intensity projection images were generated and used for determining hybridization efficiency, relative radial distances, and inter-loci distances. For each cell type analyzed for AMACR gene loci, 140 cell nuclei were quantitatively evaluated.

2.5.2 Localization Microscopy

The detailed setup of the microscope used in this study was already described elsewhere [65]. The motorized inverted TILL Photonics – FEI microscope was equipped with a Plan Apochromat 100x / 1.46 Oil, a Plan Neofluar 40 x / 0.75 Air and a Plan Neofluar Korr 20 x / 0.4 Air LD objective. Two diode lasers (405 nm; 120 mW and 642 nm; 140 mW) and two solid-state lasers (491 nm; 220 mW and 561 nm; 220 mW) were implemented with a HC BrightLine Laser Quad Set 405 / 488 / 561 / 635 mb filter. An acousto-optic tunable filter (AOTF) was used to maintain mechanical stability of the beam path while changing laser wavelength and intensity during acquisition of multi-color samples. The beam was directed into the 100 x oil immersion objective lens with a numerical aperture of NA = 1.46. The light captured by the lens was imaged onto an iXon Ultra Andor EMCCD grey scale camera. For localization microscopy, intensities of the lasers were set to maximal powers (491 nm at 2.52 kW / cm^2; 561 nm at 4.65 kW / cm^2 and 642 nm at 1.69 kW / cm^2). 2000 frames (exposure time: 100 ms per frame) were acquired for each measurement (1 cell nucleus) and each laser wavelength. For each series of SMLM experiments, typically 50 cell nuclei were registered. An in-house software (see [31, 39, 54, 65, 77, 78] for detailed descriptions) was used for the localization of signal points from blinking events in raw image stacks. The resulting data matrix containing the coordinates of detected signals was subject to further computational analysis.

3. Results

3.1 Localization of the AMACR Gene Locus in the Nucleus of Human Blood Lymphocytes

For combinatorial oligo-nucleotide FISH (COMBO-FISH) staining of the *AMACR* gene locus in interphase nuclei, a set of total 29 short oligo-nucleotide probes was used. Each oligo-nucleotide probe was labelled with an Alexa488 dye molecule at the 3´ and 5´end so that the probe set was represented by 58 dye molecules. The sequences exclusively contain homo-pyrimidines with lengths between 15 and 17 nucleotides and were entirely computationally designed. A full list of oligo-nucleotides of the probe set with their exact sequences is given in Table 1. In total, the probe

set covers 458 nucleotides of the *AMACR* gene locus, and the probes are nearly homogenously dispersed over a sequence length of about 25 kb.

Table 1 Oligo probe set used in this work for staining of the *AMACR* gene locus.

Probe ID	Length [bp]	GC content [%]	Tm* [C°]	Molar mass [g / mol]	Sequence					
AMACR1	16	43.8	40.6	6110.2	AGG	AAG	AAG	GGG	AAA	A
AMACR2	16	43.8	34.4	6110.2	GGA	GGA	AAA	GAG	AAA	G
AMACR7	15	40.0	31.2	5781.0	AGA	AAG	AAA	AGA	GGG	
AMACR9	17	35.3	30.6	6068.1	CTT	CTC	TTC	TTT	CTC	TT
AMACR10	17	58.8	45.3	6471.5	GAA	GAG	GAA	AGG	GAG	GG
AMACR11	16	37.5	37.9	5763.9	TCT	TCC	TTT	TCC	CTT	T
AMACR12	16	43.8	30.6	6110.2	GGA	GAG	AAG	AAA	GAA	G
AMACR13	17	76.5	57.9	6519.5	GGG	GGG	AAG	GGG	AGG	GA
AMACR14	15	66.7	43.3	5399.7	CCC	CTC	CCT	CTT	TCC	
AMACR16	16	62.5	45.5	5703.9	TTC	CTC	CCT	CCC	CTC	T
AMACR17	15	40.0	31.7	5459.7	TTT	CTC	CTC	TTT	TCC	
AMACR23	15	60.0	37.0	5829.0	GAG	AAG	AAG	AGG	GGG	
AMACR26	15	53.3	37.0	5813.0	AAG	GAA	GGA	AGA	GGG	
AMACR27	15	53.3	29.9	5813.0	GAA	GAG	AAG	GGA	GAG	
AMACR28	16	37.5	34.6	6094.2	AGG	GAA	AGA	AGA	AAA	G
AMACR30	15	66.7	39.9	5845.0	GAA	GAG	GGG	GGA	GAG	
AMACR31	15	53.3	34.0	5429.7	CCT	CCT	TTC	CTT	CTC	
AMACR32	16	50.0	32.9	5733.9	CTC	CTC	TTT	CTC	CTC	T
AMACR33	15	33.3	28.2	5765.0	AAA	AGA	AGG	AAA	GAG	
AMACR36	16	43.8	37.3	5748.9	TCC	CTT	TTC	TTC	TCC	T
AMACR37	17	41.2	34.1	6053.1	CTT	TCC	TCT	TCT	TTC	TC
AMACR38	17	41.2	36.9	6423.5	AGA	GAA	AGA	GGA	AAA	GG
AMACR39	17	52.9	42.2	6455.5	AGA	GGA	AGA	AAG	GGA	GG
AMACR40	16	37.5	34.6	5763.9	CTT	CTT	CCT	TCC	TTT	T
AMACR43	15	46.7	34.0	5797.0	AGA	GGA	GAA	AGG	GAA	
AMACR45	15	40.0	27.1	5459.7	CTC	TCT	CCT	TCT	TTT	
AMACR46	17	52.9	42.3	6023.1	TTT	CTC	CTC	CCC	TCT	CT
AMACR48	15	46.7	34.7	5444.7	TCT	TCT	TCC	TTT	CCC	
AMACR50	15	40.0	34.9	5781.0	AAA	AGG	GAG	GAA	AAG	

*melting temperature (median value of the denaturation curve).

Fluorescent spots of the *AMACR* gene locus in nuclei from human blood lymphocytes (one male donor), VH7, and LNCAP cells were obtained and counted in 2D maximum intensity projections of CLSM measurements. Analysis on the overall labelling statistics resulted in more than 70% (79% of lymphocytes, 93% VH7 and 71% LNCAP cells) observations with one or two *AMACR* spots (Table 2). Thereby, spots lying at the outer nuclear rim (Figure 1B; bottom left) as well as spots with very weak intensities (Figure 1B; bottom right) were excluded from analysis to avoid false positive counts.

Table 2 Statistics on oligo-nucleotide labelled spots at the *AMACR* gene locus.

Cell type	Number *n* of cells with spots	Number *n* of cells with 1 or 2 spots	Percentage [%]
Lymphocytes	92	73	79
VH7	70	65	93
LNCAP	100	71	71

The radial distribution of *AMACR* gene locus signal spots was calculated from the 3D image stack following the procedure described in [79]. Therefore, the nuclei were smoothed by a 1x3 and 3x1 binomial filter in the lateral direction and segmented using a 26-neighborhood. The intensity threshold for neighboring voxels was calculated by an iterative approach as already presented in [5].

In 76 blood lymphocyte, nuclei of relative radial distances were measured, which is defined in the range from 0% (center) to 100% (periphery) around the barycentre R_B of each nucleus as

$$R_B = \frac{\sum_i I_i r_i}{\sum_i I_i} \quad (1)$$

Where I_i is the intensity; and r_i the position of the i-th voxel. Statistical analysis resulted in a mean radial distance of 63% with the minimum radial distance measured being 8% and the maximum distance being 92% (Figure 1C). Thus, on average, spots were located more towards the nuclear periphery.

Absolute spot-to-spot distances between homologous *AMACR* gene loci were calculated in the nuclei of 38 blood lymphocyte cells as illustrated in Figure 1D. The spherical cell nuclei were selected to have the same size in order to avoid normalization problems. The calculations resulted in a mean distance of 7.7 µm with minimum and maximum distances of 2.1 µm and 18.4 µm, respectively (Figure 1E). About 24% of spot pairs are separated by an absolute distance d of 12 µm (the most frequent distance), and only very few spots lie 14 to 18 µm apart from each other.

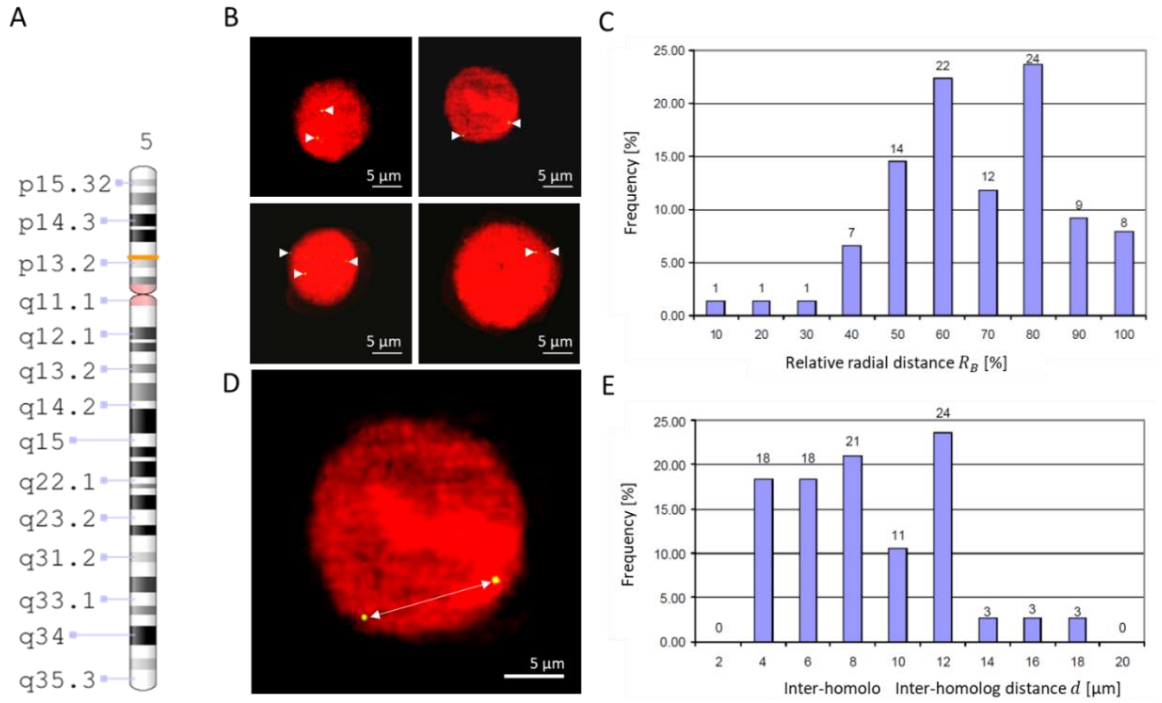

Figure 1 COMBO-FISH signal spots at the *AMACR* gene locus in interphase chromatin of human blood lymphocytes. (A) Idiogram of human chromosome 5 with the *AMACR* locus (orange band). (B) 2D maximum intensity projections along the z-axis after CLSM measurements of example lymphocyte interphase nuclei with COMBO-FISH staining of *AMACR* gene labelling (green) by an appropriate oligo-nucleotide probe set. Counterstaining of nuclei was performed with TOPRO-3-iodide (red). Cells can have two (top), three (bottom left), or one bright and one weak (bottom right) signal spots in the image plane. (C) Histogram of relative radial distances of signal spots from the nuclear center (number of bins 10, bin width = 10). (D) Example cell with two signal spots that was used for inter-homolog distance measurements. (E) Histogram of inter-homolog distances measured in interphase nuclei (number of bins 10, bin width = 10).

3.2 Localization of Genomic Alu Elements and Chromosome 9 Centromeres

Specific labelling of *Alu* elements and chromosome 9 centromeres (C9) in SkBr3 cells was successfully performed with short oligo-nucleotide probes according to the COMBO-FISH method for the analysis of nuclear architecture via SMLM. Point-like clusters of fluorescence signals from chromosome 9 centromere labelling were clearly visible by means of fluorescence microscopy (Figure 2A, B) and after super-resolution localization microscopy (Figure 2C). In contrast, *Alu* fluorescent labels were distributed over the whole nucleus except at the *Alu*-free nuclear rim, which was already observed in past studies using conventional FISH probes [4]. Wide-field overview images of typical region of interests (ROIs) that were used for localization microscopy are presented for two example cell nuclei in Figure 2B. These images suggest a complete co-localization between the DAPI staining and the *Alu* labelling due to the diffraction induced image spreading. By quantitative evaluation of SMLM data, this visual misinterpretation could be avoided.

Density images were computed with in-house software according to [65] with pixel intensities corresponding to the number of signal points counted inside a radial distance of 1000 nm around a pixel. A 50-nm Gaussian filter was applied to facilitate visual recognition of structural arrangements. Clusters of points referring to one centromere 9 were identified based on the criterion of a minimum number of 40 labelling points inside a 200-nm radius around a cluster centroid with in-house software as described in [31, 54, 80].

A super resolution overlay image comprised of *Alu* signal densities and a centromere 9 obtained from localization microscopy measurements of one example cell section is shown in Figure 2C. Instead of a homogenous signal all over the nucleus as observed from conventional fluorescence microscopy, fluorescent points of *Alu* signals are non-randomly distributed over the whole nucleus. This pointillist image demonstrates the differing point densities in the *Alu* distribution pattern. Some regions with high *Alu* signal densities overlay with the centromere 9 point cluster.

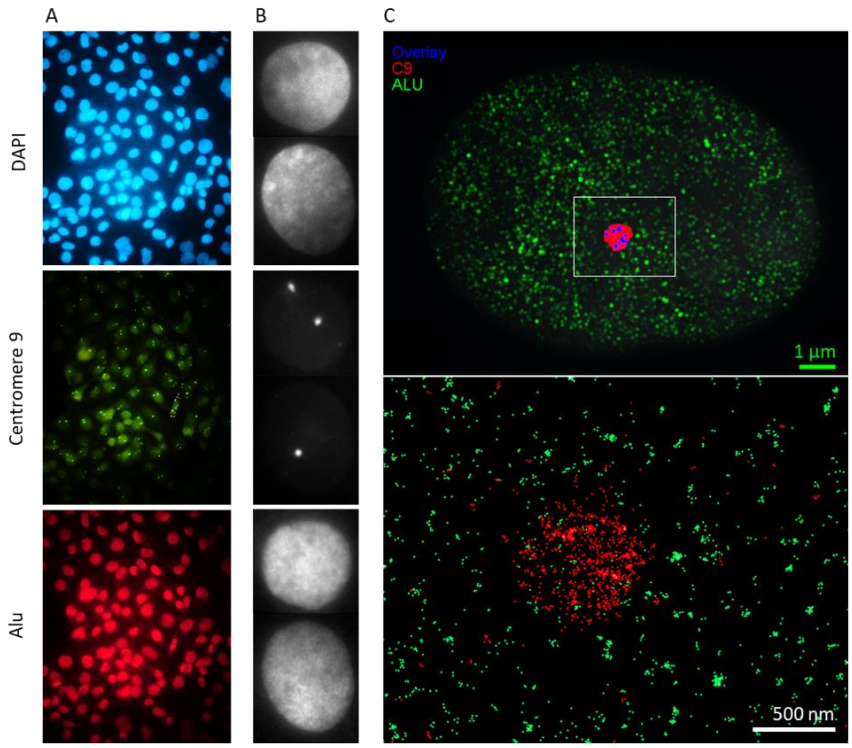

Figure 2 Diffraction limited and super resolution images of *Alu* and chromosome 9 centromere signals. (A) Epifluorescence overview image showing successful staining of chromosome 9 (middle) centromeres and genomic *Alu* (bottom) and DAPI counterstaining (top). Note: Due to the low magnification and low numerical aperture of these images, the camera gain has to be maximized leading, in general, to a color background; although, the specimen preparation was nearly background-free as shown in B. (B) Diffraction-limited image sections of typical region of interests for two example cells. (C) Super-resolution overlay image of Alu densities (green), a centromere 9 points cluster (red), and overlaying regions (blue). Note: In (C), only one image plane (no projection) is shown, where one centromere 9 is located. A magnified point coordinate representation of the white box is shown below.

Computational probe design allows estimates about the theoretical probe binding sites on the human reference genome. Figure 3C shows an idiogram of chromosome 9 with the distribution of its *Alu* probe binding sites (red) and *Alu* consensus sequences (blue). For the *Alu* probe used in this study, a total number of 401,133 probe binding sites were found for the whole genome, of which 16,459 sites (4.1%) lie on chromosome 9. From this fraction, a hypothetical number of measured *Alu* localization signals assumed to originate from chromosome 9 can be simply back calculated. For the example cell in Figure 2C, 15,887 total *Alu* signals were measured, which results in 652 (4.1%) signals that were presumably detected from genomic *Alu* labels on chromosome 9 (Table 3).

The radius of a circle centered at the centromere 9 centroid can be defined at which the theoretical number of chromosome 9 related *Alu* signals is included inside the circle boundaries. This could be a most simple estimate for the circular approximation of a chromosome 9 territory merely derived from the location of its centromere and the spatial distribution of *Alu* localization signals inside the nucleus. In fact, our calculations resulted in circular territories of plausible sizes when compared to the whole nucleus (Figure 3A and magnification in B). As each SMLM

measurement results in a distinct number of total *Alu* signals for each individual cell, different radii could be calculated for each single centromere centroid.

Table 3 *Alu* probe binding sites on chromosome 9 of the reference genome and hypothetical *Alu* localization signals originating from chromosome 9.

Region	*Alu* probe binding sites	*Alu* localization signals*
chromosome 9	16,459	652
whole genome	401,133	15,887
fraction	0.0410	0.0410

*Calculations were based on the example cell shown in Figure 2C.

The average distribution of *Alu* signal points around 38 centromere 9 cluster centroids were calculated. Higher and lower densities of *Alu* signals can be observed over certain radial distances from the centromere 9 cluster centroid (Figure 3D). In fact, varying densities of *Alu* elements (blue) as well as probe binding sites (red) can also be mapped along the full length of the human chromosome 9 reference genome, as depicted in Figure 3C.

We calculated the theoretical chromosome 9 territory radii around 38 centromere centroids in 20 cell nuclei. Our analysis revealed that centromere 9 point clusters tend to divide into two subpopulations (Figure 4A). Manual evaluation revealed that larger radii belong to centromere 9 point clusters located at the nuclear periphery, whereas smaller radii were derived from centromere 9 point clusters that lie in the inner areas of the nucleus (Figure 4C-F). This observation could be also confirmed by measuring the relative radial distances of centromere 9 cluster centroids and comparing them against the calculated radii of putative chromosome 9 territories (Figure 4B). It can be seen that the largest radii (ranging from 1800 to 2400 nm) are located in a relatively narrow margin at the nuclear periphery (dark red dots), while smaller radii (ranging from 1200 to 1800 nm) are distributed over a wider range from the nuclear center towards the periphery (light orange dots). In both cases (Figure 4A and B), a skewedness of the distribution of chromosome 9 radii is observable.

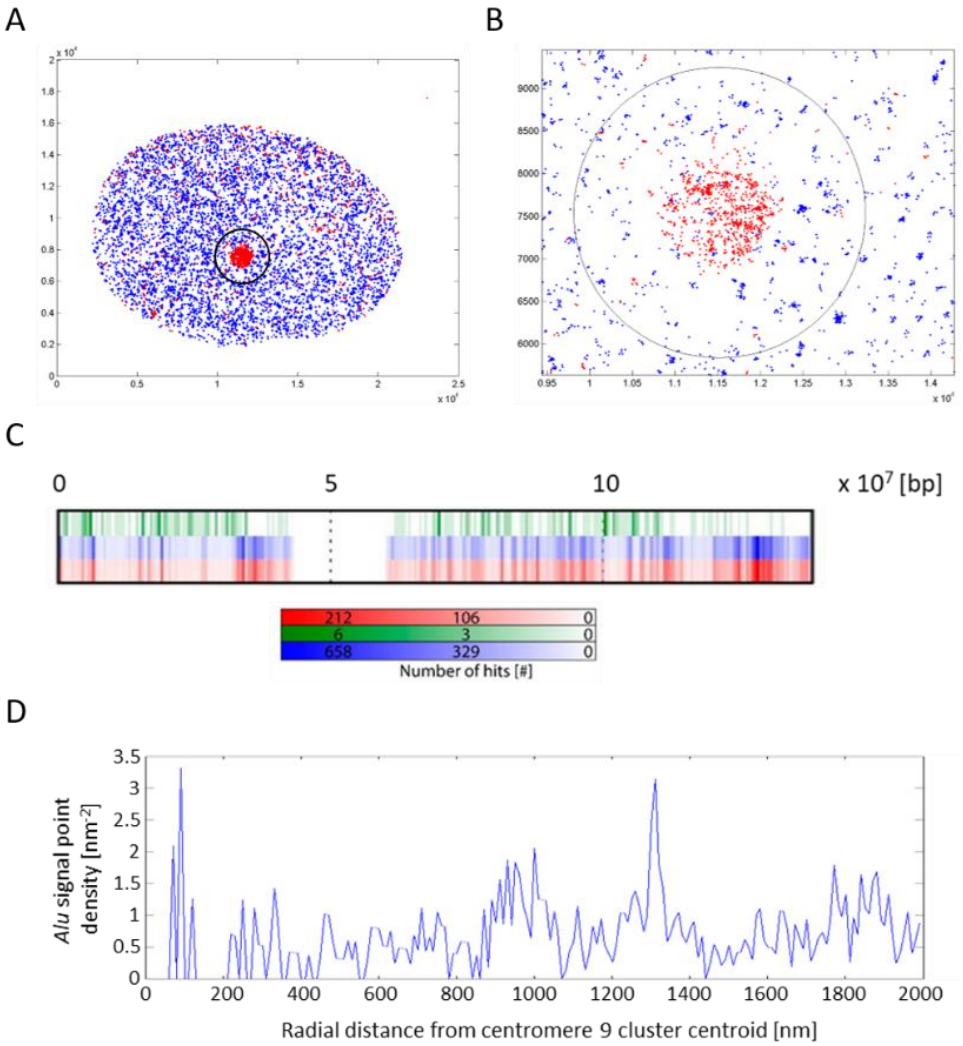

Figure 3 Estimates of chromosome 9 architecture by its centromere and genomic Alu. (A) Plot of the raw point matrix obtained from SMLM data of example cell in Figure 2C. A circular approximation of a chromosome 9 territory (black circle) modelled from the theoretical distribution of *Alu* elements (blue dots) around the chromosome 9 centromere (red dots). (B) Magnification of the region of interest in (A). (C) Idiogram of chromosome 9 showing the positional distribution of *Alu* probe binding sites (red), *Alu* consensus sequences (blue), and binding sites of a probe against genomic L1 elements (green). (D) The radial distribution of *Alu* signal points around a centromere 9 cluster centroid averaged over 38 centromere 9 clusters.

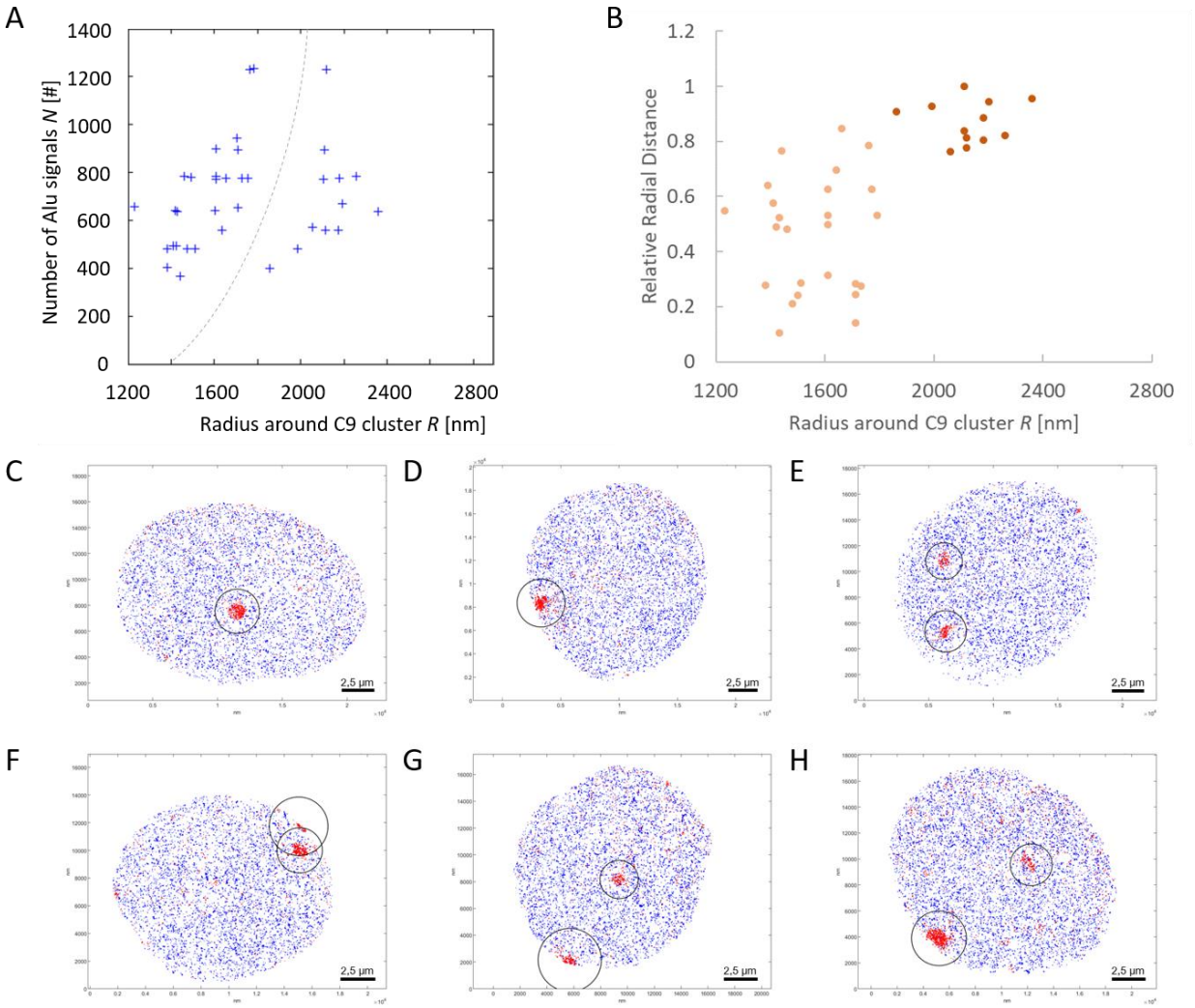

Figure 4 Nuclear localization of centromere 9 alleles. (A) Radii and *Alu* signal number boundary conditions of each individual centromere centroid. The grey dotted curve illustrates two subpopulations of chromosome 9 centromeres. (B) Radii around centromere 9 cluster centroid plotted against their relative radial distances. Light orange and dark red dots represent those centromeres on the left and right side of the dotted line in the plot in (A), respectively. (C-H) Example nuclei showing differently positioned chromosome 9 centromeres (center) inside the nucleus.

3.3 Three-Colour Super-Resolution Microscopy of Genomic Alu, L1 and H3K9me3 Heterochromatin Marks in the Same Nucleus

Genomic *Alu* sequences, L1 sequences, and H3K9me3 were labelled by a combination protocol consisting of COMBO-FISH and immunostaining that was established in [65].

The oligo-nucleotide sequence (*GGTGATTTCTGCATTTC*) for the L1 probe was recently designed in our group by a “sliding window” approach [80] and had already described in [65]. The binding sites of the L1 probe compared to the distribution of *Alu* consensus sequences and the *Alu* probe binding sites on chromosome 9 can be seen in Figure 3C.

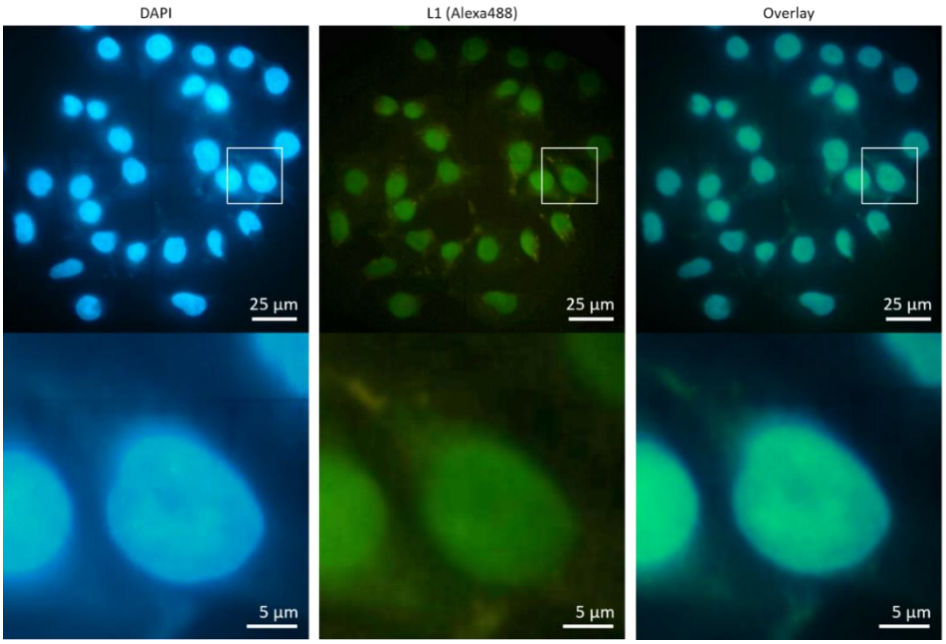

Figure 5 Low temperature L1 oligo-nucleotide FISH on SkBr3 cells. L1 elements could be successfully labelled by the new oligo-nucleotide probe (Alexa Fluor® 488-*GGTGATTTCTGCATTTC)* at low temperature conditions, which is a main requirement for combination with immunostaining. Building up on these preliminary results, a combined three-color staining of L1 together with *Alu* and H3K9me3 could be realized (see below). The left row of images shows the DAPI counterstaining of the cell ensemble, whereas the middle row of images shows the L1 oligo-nucleotide label signals as obtained by standard epifluorescence microscopy. Overlays of both channels (right column) show that L1 signals are distributed all over the nucleus and correlate with DAPI. Bottom images are magnifications of selected regions (white boxes) of the corresponding top images.

Initial experiments demonstrated that the new L1 oligo-nucleotide probe can be applied at the same low temperature conditions and with the exact same protocol as those for the *Alu* probe (Figure 5). Using these preliminary results, oligo-nucleotide labelling of L1 together with Alu could be combined with antibody labelling of heterochromatin marker H3K9me3.

Figure 6 contains the results obtained by SMLM of a SkBr3 cell nucleus specifically labelled for genomic *Alu* and L1 by the two different uniquely binding oligo-nucleotides and for heterochromatin by antibodies specific against the histone methylation site H3K9me3. Wide-field images (Figure 6A) show fluorescence signals distributed over the whole nucleus, which can be validated by DAPI counterstaining. Micrometer-sized regions of higher signal intensity are typically visible for H3K9me3, whereas *Alu* signals are more homogenously distributed, as already mentioned above. L1 staining shows few large areas with decreased signal intensity in the midst of homogenous signals. Such areas could not be observed in the other staining regions or by DAPI staining, but regions of high H3K9me3 intensity seem to overlay with them. Localization density images (Figure 6B) highlight dense accumulations of localization events. Here, it is observable that H3K9me3 tags representing methylated heterochromatin are distributed in denser but fewer accumulations, whereas *Alu* signals are more evenly distributed throughout the nucleus and

arranged in less dense accumulations. L1 density images show characteristics of both, as they seem to be organized in dense accumulations that are restricted to smaller regions, as observed for H3K9me3, but are also homogenously present over large regions of the nucleus like *Alu*. The composite of all three density images (Figure 6C) shows regions with pair-wise occurrences of high signals density and areas where dense accumulations of *Alu*, L1, and H3K9me3 occur together.

Super-resolution SMLM images (Figure 6C) reveal that the signal dense regions in density images are further comprised of finer structures. Even at the nano-scale, H3K9me3 seems to be predominantly accumulated in relatively large well-separated globular formations (magenta boxes). Some *Alu* signals are also arranged in such globular formations, but most *Alu* signals are organized into smaller nanostructures that are either point-like or, sometimes, even have a rod-shaped form (red boxes). Compared to H3K9me3 and *Alu*, L1 nanostructures are more heterogeneous in size, shape, and spatial arrangement. On several occasions, several L1 nanostructures were observed to be aligned in a fiber-like manner resembling beads on a string (green boxes), which did not occur for either H3K9me3 or *Alu*.

Spatial analyses of three-color SMLM data resulted in distinct local maxima in each of the Ripley's K statistics in the sub-diffraction nanometer distance range (Figure 7). *Alu* signals show a characteristic peak around 15 nm, whereas L1 and H3K9me3 signals similarly have local maxima at about a 20-nm distance value. Based on these findings, L1 and H3K9me3 might share similar structural features or chromatin compartments, which differ from the *Alu* representing chromatin nanostructure.

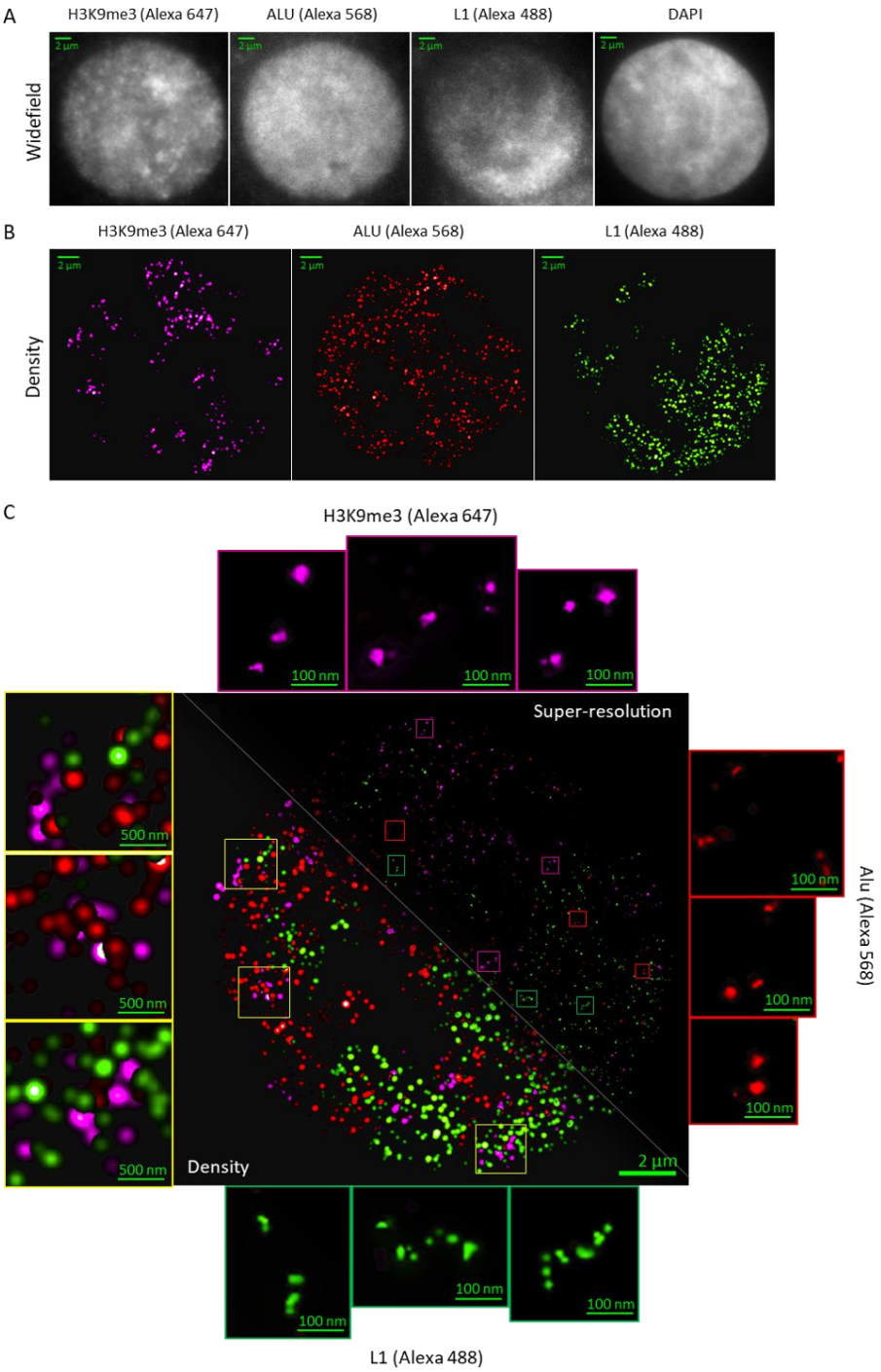

Figure 6 Three-color super-resolution images of *Alu*, L1, and H3K9me3. (A) Wide-field images at diffraction limited resolution were taken to obtain a first overview of the nucleus and the region of interest (ROI) that was subsequently subjected to localization microscopy. Note: Since specific COMBO-FISH labelling works background-free, the wide-field images are oversaturated in order to visualize the cell nucleus completely. (B) Density images are generated from the pointillist matrix of localization signals for highlighted visualization of regions with distinct signal densities. (C) Density and super-resolution SMLM overlay images and their magnifications show regions with different combinations of co-localization on the microscopic level (yellow boxes) and characteristic nanostructures of H3K9me3 marks (magenta), genomic *Alu* (red), and genomic L1 (green).

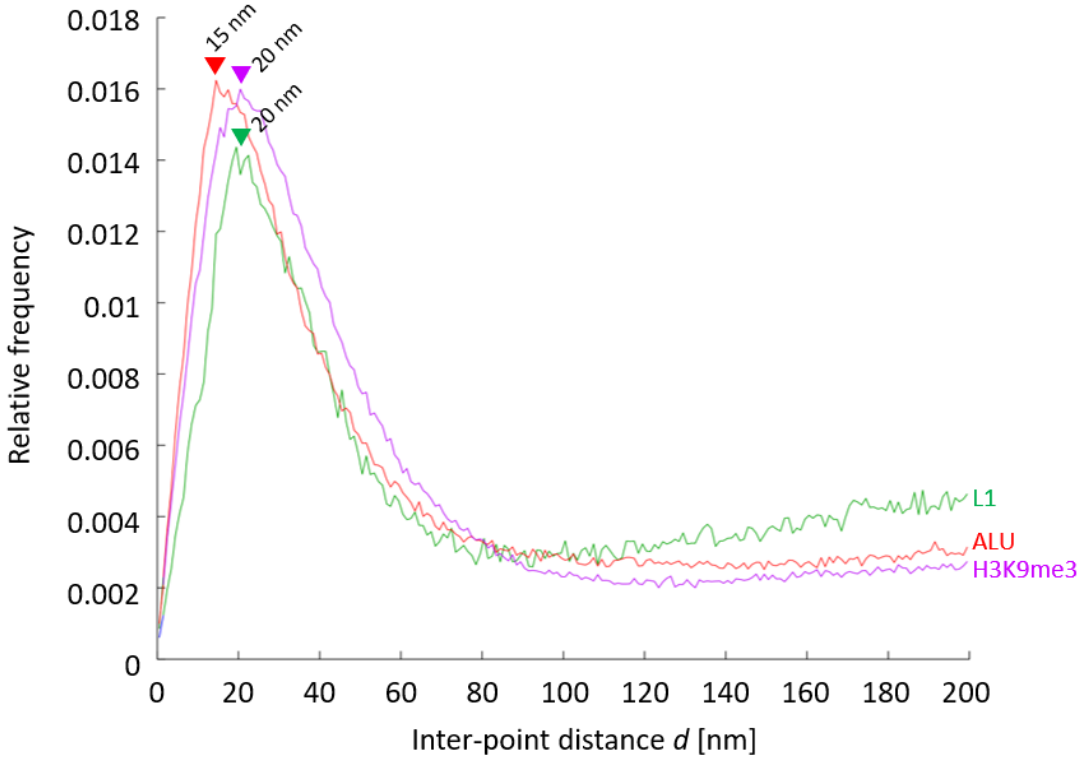

Figure 7 Spatial SMLM data analysis by Ripley's K statistics for the *Alu*, L1, and H3K9me3 triple staining. All three chromatin markers show distinct peaks in their Ripley's K statistics. The frequency of *Alu* inter-point distances (red) has a local maximum at around 15 nm, whereas L1 (green) and H3K9me3 (magenta) result in local maxima around 20 nm point-to-point distances.

4. Discussion

The application of FISH has become an indispensable tool in modern bio-medical research and medical diagnosis using fluorescence microscopy and imaging in advanced procedures. Modern molecular biology offers a plethora of probes and commercially available ready-to-use FISH labelling kits. Nearly all of the FISH protocols applied so far make use of a thermal target and probe denaturation supported by the application of chaotropic agents like formamide. Beyond an additional influence on the target morphology [46, 47], the denaturation step hinders the simultaneous combination of FISH labelling with antibody-based labelling of native protein structures. Moreover, in many cases, very special targets have to be labelled, or species are investigated for which common FISH probes are not available. In this work, oligo-nucleotide approaches for specific FISH labelling are a method of choice.

COMBO-FISH [53], as one of the established oligo-nucleotide techniques, offers the opportunity to circumvent several drawbacks of standard FISH protocols and reduces the wet laboratory work considerably. The COMBO-FISH probe sets are completely computer designed and can be developed for any given genomic region in any sequenced species. This makes the technique highly flexible [55], thereby strictly focusing labelling on the given target without considerable overlaps that could occur from using standard FISH probes. Since the probes are completely designed by a computer data search, additional parameters, such as binding energy, Watson-Crick or Hoogsteen bonding, probe length, etc. [61], could be considered for the final combination of

probes. Finally, target denaturation can be avoided or minimized [65] so that a combination with immunostaining and SMLM becomes feasible [31]. This offers novel perspectives for investigations of chromatin nano-architecture by super-resolution microscopy in normal and cancer cells.

In this article, we have shown two typical examples for the application of COMBO-FISH in order to demonstrate potential applications. The probe combination specifically co-localizing in the *AMACR* region has allowed measurement of the radial distribution of the respective gene target site in different cell lines. Although it has been shown that COMBO-FISH can have a hybridization efficiency of 99% of the target sites [56], this has not been realized here since the *AMACR* region is labelled by only 29 oligo-stretches, i.e. only by 58 dye molecules. This may be due to fluorescence at the detection limit of the confocal microscope that was used, even though the preparation protocol had been optimized to nearly no unspecific fluorescence background (leading to high signal/background ratio). However, the local conditions on a slide might have been responsible to reduce the brightness of an *AMACR* spot so that it had not been considered for further quantitative analysis. This shortcoming could be overcome by SMLM and the detection of single dye molecules.

On the other hand, it should be considered that for VH7 cells with a normal karyotype, 93% of the results reflected two chromosomes 5, whereas 29% of the cells showed more than 2 signals for LNCAP, which could be tri- or tetraploid. Nevertheless, on average, more than 77% of the labelling sites could be used for further processing. Depending on the research question addressed, this may be sufficient or overcome by additional measurements and selection of only completely labelled nuclei.

Relative radial distances were calculated for *AMACR* fluorescence signals in lymphocyte nuclei and resulted in an overall localization of the gene locus (63%) more towards the nuclear periphery, which is in concordance with earlier findings on the peripheral location of the relatively large and gene dense chromosome 5 territory [4, 19, 81, 82]. The data also suggest that the two homologues may be positioned slight differently, if one refers to the two maxima at 60% and 80% radius. Moreover, our study provides ground-breaking data on the inter-loci distances of the *AMACR* gene in interphase nuclei of lymphocytes. With a mean distance of 7.7 µm, the homologous *AMACR* genes are relatively far apart from each other, as usually assumed for homologous genes or chromosomes [82].

In order to improve the detection efficiency and to enter the meso- and nano-scale of chromatin architecture, SMLM can be applied [31, 54, 56, 65]. Alignment free search routines for uniquely binding oligo-nucleotides [65, 83] offer new perspectives to better understand the overall organization of chromatin and the effects of transposable and repetitive elements so far a highly challenging and controversial field of research [84-89]. The examples presented here demonstrate the capacity of SMLM in combination with COMBO-FISH to quantify the topology of chromatin organization. This can be supported by improved labelling combinations of COMBO-FISH and immunostaining. Such measurements on the single molecule level resolve co-localizing signals to closely neighboring signals and allow the quantification of single molecule arrangements.

Our examples show that centromere probes are in close vicinity to *Alu* probes. Indeed, many transposable elements were also found to be interspersed into the satellite tandem arrays of centromeres [90, 91] and in pericentromeric regions [92-94] and might play important roles in centromere evolution [91] and function [95, 96]. It is also pertinent to mention that the nano-scale co-localizations indicated in our data can also arise due to the size of the labelling tags that may

lead the dye molecules to such a close vicinity (typically 15 nm or below) that they lie below the separation limit of the SMLM data algorithms used. Yet, the labelled target structures must lie at certain distances apart, depending on probe sizes and accuracy of SMLM localization that altogether still lie far below diffraction limited resolutions. This demonstrates the capabilities of COMBO-FISH in combination with SMLM, which enables multi-parametric analysis of nuclear structures and functions on the nano-scale.

Our data representing the "*Alu*-network" in the cell nucleus allow an estimation of the chromosome territory size (about 4% of the signals) around the centroid of a centromere. Assuming that the labelling efficiency and detection efficiency do not vary between individual cell nuclei, the data reflect a different compaction of the chromosome 9 territories, whether they belong to more centrally located or the more peripherally located allele. The effect that homologous chromosome territories slightly differ in their sizes might not be surprising; the more surprising effect may be that the rough evaluation of SMLM data reflects this difference unambiguously.

Furthermore, SMLM analysis of nuclei that were labelled by two COMBO-FISH probes for *Alu* and L1 in combination with antibodies against H3K9me3 heterochromatin was successfully performed. Analyses reveal how each chromatin landmark exhibits its own characteristic feature with respect to their nano-architecture. L1 specific and *Alu* specific probes as well as H3K9me3 specific antibodies formed cluster-like structures with representative characteristics for each type of chromatin mark. Thereby, heterochromatin labelling tags by H3K9me3 antibodies form joint clusters with both L1 and *Alu* clusters, and regions with simultaneous presence of all three chromatin structures at close proximity were observable. Ripley's K based spatial analysis revealed an enrichment of inter-point distances in the lower nanometer range for all three markers (Figure 7). Interestingly, L1 and H3K9me3 spatial analysis resulted in highly similar features, thus providing evidence that they both might share similar chromatin nano-architectures that are, again, distinct from the *Alu* chromatin nano-environment. These results are in concordance with past findings that reveal L1 elements are enriched in inactive heterochromatic regions, whereas *Alu* elements are also highly present in active genomic regions. Follow-up studies will investigate the isolated and interconnected properties of multiple chromatin markers inside a single nucleus, as presented in this work, and will further elevate our knowledge about genome nano-architecture and its complex functions.

In conclusion, the data presented in this article demonstrate typical and potential applications of COMBO-FISH in future investigations and its high variations of labelling. Combining this method with super-resolution recording and quantification approaches may contribute to a better understanding of genome architecture and mechanisms driven by topology and modifications of native chromatin structure.

5. Conclusions

Fluorescence microscopy of small nano-tags has become a powerful tool to study intact genome architecture and organization. In this work, we confirmed that COMBO-FISH labelling, together with both conventional and super-resolution fluorescence microscopy, can be applied to a variety of genomic targets for genome architecture research on the micro-, meso-, and nano-scales. By studying chromatin landmarks like gene loci, centromeres, repetitive elements, and

histone marks, we could identify well-suited parameters to describe spatial organization in the nucleus from the micro- to nano-scale. We hope that this work motivates future research on COMBO-FISH and demonstrates that this labelling technique in combination with immunostaining may become a powerful tool for a wide spectrum of research-driven combinations of labelling.

Acknowledgments

The authors thank Jutta Schwarz-Finsterle for continuous discussions and support of the work of Florence Laure Djikimi Tchetgna. Further, the authors would like to thank Georg Hildenbrand and Götz Pilarczyk for fruitful discussions and their continuous scientific support. Finally, the never ending, lively stimulations by Cornelia-Corinna Seegler-Sandbanck, European Institute of Feasiblity Studies, Strasburg are acknowledged.

Author Contributions

Jin-Ho Lee performed the experiments with low temperature COMBO-FISH and SMLM and wrote the manuscript. Florence Laure Djikimi Tchetgna carried out the experiments with COMBO-FISH for *AMACR*. Matthias Krufczik and Jin-Ho Lee developed the low temperature COMBO-FISH technique. Eberhard Schmitt designed the *AMACR* probe set. Christoph Cremer and Felix Bestvater supported by equipment. Michael Hausmann supervised Jin-Ho Lee and Matthias Krufczik and wrote the manuscript.

Competing Interests

The authors have declared that no competing interests exist.

References

1. Schmitt AD, Hu M, Ren B. Genome-wide mapping and analysis of chromosome architecture. Nat Rev Mol Cell Biol. 2016; 17: 743-755.
2. Pombo A, Dillon N. Three-dimensional genome architecture: players and mechanisms. Nat Rev Mol Cell Biol. 2015; 16: 245-257.
3. Woodcock CL. Chromatin architecture. Curr Opin Struct Biol. 2006; 16: 213-220.
4. Bolzer A, Kreth G, Solovei I, Koehler D, Saracoglu K, Fauth C, et al. Three-dimensional maps of all chromosomes in human male fibroblast nuclei and prometaphase rosettes. PLoS Biol. 2005; 3: e157.
5. Cremer T, Cremer C. Chromosome territories, nuclear architecture and gene regulation in mammalian cells. Nat Rev Genet. 2001; 2: 292-301.
6. Cremer T, Kurz A, Zirbel R, Dietzel S, Rinke B, Schrock E, et al. Role of chromosome territories in the functional compartmentalization of the cell nucleus. Cold Spring Harb Symp Quant Biol. 1993; 58: 777-792.
7. Cremer T, Kreth G, Koester H, Fink RH, Heintzmann R, Cremer M, et al. Chromosome territories, interchromatin domain compartment, and nuclear matrix: an integrated view of the functional nuclear architecture. Crit Rev Eukaryot Gene Expr. 2000; 10: 179-212.
8. Bickmore WA, van Steensel B. Genome architecture: domain organization of interphase chromosomes. Cell. 2013; 152: 1270-1284.

9. Rouquette J, Cremer C, Cremer T, Fakan S. Functional nuclear architecture studied by microscopy: present and future. Int Rev Cell Mol Biol. 2010; 282: 1-90.
10. Falk M, Hausmann M, Lukasova E, Biswas A, Hildenbrand G, Davidkova M, et al. Determining Omics Spatiotemporal Dimensions Using Exciting New Nanoscopy Techniques to Assess Complex Cell Responses to DNA Damage: Part B− Structuromics. 2014; 24: 225-247.
11. Cremer M, von Hase J, Volm T, Brero A, Kreth G, Walter J, et al. Non-random radial higher-order chromatin arrangements in nuclei of diploid human cells. Chromosome Res. 2001; 9: 541-567.
12. Cremer T, Cremer M, Dietzel S, Muller S, Solovei I, Fakan S. Chromosome territories--a functional nuclear landscape. Curr Opin Cell Biol. 2006; 18: 307-316.
13. Cremer M, Schmid VJ, Kraus F, Markaki Y, Hellmann I, Maiser A, et al. Initial high-resolution microscopic mapping of active and inactive regulatory sequences proves non-random 3D arrangements in chromatin domain clusters. Epigenetics Chromatin. 2017; 10: 39.
14. Neusser M, Schubel V, Koch A, Cremer T, Muller S. Evolutionarily conserved, cell type and species-specific higher order chromatin arrangements in interphase nuclei of primates. Chromosoma. 2007; 116: 307-320.
15. Dekker J, Belmont AS, Guttman M, Leshyk VO, Lis JT, Lomvardas S, et al. The 4D nucleome project. Nature. 2017; 549: 219-226.
16. Wachsmuth M, Caudron-Herger M, Rippe K. Genome organization: balancing stability and plasticity. Biochim Biophys Acta. 2008; 1783: 2061-2079.
17. Misteli T. Beyond the sequence: cellular organization of genome function. Cell. 2007; 128: 787-800.
18. Lanctot C, Cheutin T, Cremer M, Cavalli G, Cremer T. Dynamic genome architecture in the nuclear space: regulation of gene expression in three dimensions. Nat Rev Genet. 2007; 8: 104-115.
19. Kozubek S, Lukasova E, Jirsova P, Koutna I, Kozubek M, Ganova A, et al. 3D Structure of the human genome: order in randomness. Chromosoma. 2002; 111: 321-331.
20. de Wit E, de Laat W. A decade of 3C technologies: insights into nuclear organization. Genes Dev. 2012; 26: 11-24.
21. Denker A, de Laat W. The second decade of 3C technologies: detailed insights into nuclear organization. Genes Dev. 2016; 30: 1357-1382.
22. Lieberman-Aiden E, van Berkum NL, Williams L, Imakaev M, Ragoczy T, Telling A, et al. Comprehensive mapping of long-range interactions reveals folding principles of the human genome. Science. 2009; 326: 289-293.
23. Dekker J, Rippe K, Dekker M, Kleckner N. Capturing chromosome conformation. Science. 2002; 295: 1306-1311.
24. Dostie J, Richmond TA, Arnaout RA, Selzer RR, Lee WL, Honan TA, et al. Chromosome Conformation Capture Carbon Copy (5C): A massively parallel solution for mapping interactions between genomic elements. Genome Research. 2006; 16: 1299-1309.
25. Rao SSP, Huntley MH, Durand NC, Stamenova EK, Bochkov ID, Robinson JT, et al. A 3D map of the human genome at kilobase resolution reveals principles of chromatin looping. Cell. 2014; 159: 1665-1680.
26. Dixon JR, Selvaraj S, Yue F, Kim A, Li Y, Shen Y, et al. Topological domains in mammalian genomes identified by analysis of chromatin interactions. Nature. 2012; 485: 376-380.

27. Shen Y, Yue F, McCleary DF, Ye Z, Edsall L, Kuan S, et al. A map of the cis-regulatory sequences in the mouse genome. Nature. 2012; 488: 116-120.
28. Nora EP, Lajoie BR, Schulz EG, Giorgetti L, Okamoto I, Servant N, et al. Spatial partitioning of the regulatory landscape of the X-inactivation centre. Nature. 2012; 485: 381-385.
29. de Laat W, Duboule D. Topology of mammalian developmental enhancers and their regulatory landscapes. Nature. 2013; 502: 499-506.
30. Sati S, Cavalli G. Chromosome conformation capture technologies and their impact in understanding genome function. Chromosoma. 2017; 126: 33-44.
31. Hausmann M, Ilic N, Pilarczyk G, Lee JH, Logeswaran A, Borroni AP, et al. Challenges for super-resolution localization microscopy and biomolecular fluorescent nano-probing in cancer research. Int J Mol Sci. 2017; 18.
32. Cremer C, Masters BR. Resolution enhancement techniques in microscopy. The European Physical Journal H. 2013; 38: 281-344.
33. Betzig E, Patterson GH, Sougrat R, Lindwasser OW, Olenych S, Bonifacino JS, et al. Imaging intracellular fluorescent proteins at nanometer resolution. Science. 2006; 313: 1642-1645.
34. Hess ST, Girirajan TP, Mason MD. Ultra-high resolution imaging by fluorescence photoactivation localization microscopy. Biophys J. 2006; 91: 4258-4272.
35. Rust MJ, Bates M, Zhuang X. Sub-diffraction-limit imaging by stochastic optical reconstruction microscopy (STORM). Nat Methods. 2006; 3: 793-795.
36. Heilemann M, van de Linde S, Schuttpelz M, Kasper R, Seefeldt B, Mukherjee A, et al. Subdiffraction-resolution fluorescence imaging with conventional fluorescent probes. Angew Chem Int Ed Engl. 2008; 47: 6172-6176.
37. Folling J, Bossi M, Bock H, Medda R, Wurm CA, Hein B, et al. Fluorescence nanoscopy by ground-state depletion and single-molecule return. Nat Methods. 2008; 5: 943-945.
38. Dertinger T, Colyer R, Iyer G, Weiss S, Enderlein J. Fast, background-free, 3D super-resolution optical fluctuation imaging (SOFI). P Natl Acad Sci USA. 2009; 106: 22287-22292.
39. Lemmer P, Gunkel M, Baddeley D, Kaufmann R, Urich A, Weiland Y, et al. SPDM: light microscopy with single-molecule resolution at the nanoscale. Appl Phys B-Lasers O. 2008; 93: 1-12.
40. Bohn M, Diesinger P, Kaufmann R, Weiland Y, Muller P, Gunkel M, et al. Localization microscopy reveals expression-dependent parameters of chromatin nanostructure. Biophys J. 2010; 99: 1358-1367.
41. Zhang Y, Mate G, Muller P, Hillebrandt S, Krufczik M, Bach M, et al. Radiation induced chromatin conformation changes analysed by fluorescent localization microscopy, statistical physics, and graph theory. PLoS One. 2015; 10: e0128555.
42. Bauman JG, Wiegant J, Borst P, van Duijn P. A new method for fluorescence microscopical localization of specific DNA sequences by in situ hybridization of fluorochromelabelled RNA. Exp Cell Res. 1980; 128: 485-490.
43. Hausmann M, Cremer C, Linares-Cruz G, Nebe TC, Peters K, Plesch A, et al. Standardisation of FISH-procedures: summary of the Second Discussion Workshop. Cell Oncol. 2004; 26: 119-124.
44. Braz GT, He L, Zhao H, Zhang T, Semrau K, Rouillard JM, et al. Comparative Oligo-FISH mapping: An efficient and powerful methodology to reveal karyotypic and chromosomal evolution. genetics. 2018; 208: 513-523.

45. Wolf D, Rauch J, Hausmann M, Cremer C. Comparison of the thermal denaturation behaviour of DNA-solutions and metaphase chromosome preparations in suspension. Biophys Chem. 1999; 81: 207-221.
46. Rauch J, Wolf D, Hausmann M, Cremer C. The influence of formamide on thermal denaturation profiles of DNA and metaphase chromosomes in suspension. Z Naturforsch C. 2000; 55: 737-746.
47. Winkler R, Perner B, Rapp A, Durm M, Cremer C, Greulich KO, et al. Labelling quality and chromosome morphology after low temperature FISH analysed by scanning far-field and near-field optical microscopy. J Microsc. 2003; 209: 23-33.
48. Lander ES, Linton LM, Birren B, Nusbaum C, Zody MC, Baldwin J, et al. Initial sequencing and analysis of the human genome. Nature. 2001; 409: 860-921.
49. Beliveau BJ, Apostolopoulos N, Wu CT. Visualizing genomes with Oligopaint FISH probes. Curr Protoc Mol Biol. 2014; 105: Unit 14 23.
50. Beliveau BJ, Joyce EF, Apostolopoulos N, Yilmaz F, Fonseka CY, McCole RB, et al. Versatile design and synthesis platform for visualizing genomes with Oligopaint FISH probes. Proc Natl Acad Sci U S A. 2012; 109: 21301-21306.
51. Yamada NA, Rector LS, Tsang P, Carr E, Scheffer A, Sederberg MC, et al. Visualization of fine-scale genomic structure by oligonucleotide-based high-resolution FISH. Cytogenet Genome Res. 2011; 132: 248-254.
52. Boyle S, Rodesch MJ, Halvensleben HA, Jeddeloh JA, Bickmore WA. Fluorescence in situ hybridization with high-complexity repeat-free oligonucleotide probes generated by massively parallel synthesis. Chromosome Res. 2011; 19: 901-909.
53. Hausmann M, Winkler R, Hildenbrand G, Finsterle J, Weisel A, Rapp A, et al. COMBO-FISH: specific labeling of nondenatured chromatin targets by computer-selected DNA oligonucleotide probe combinations. Biotechniques. 2003; 35: 564-570, 572-567.
54. Stuhlmuller M, Schwarz-Finsterle J, Fey E, Lux J, Bach M, Cremer C, et al. In situ optical sequencing and structure analysis of a trinucleotide repeat genome region by localization microscopy after specific COMBO-FISH nano-probing. Nanoscale. 2015; 7: 17938-17946.
55. Schmitt E, Wagner J, Hausmann M. Combinatorial selection of short triplex forming oligonucleotides for fluorescence in situ hybridisation COMBO-FISH. J Comput Science. 2012; 3: 328-334.
56. Müller P, Schmitt E, Jacob A, Hoheisel J, Kaufmann R, Cremer C, et al. COMBO-FISH enables high precision localization microscopy as a prerequisite for nanostructure analysis of genome loci. Int J Mol Sci. 2010; 11: 4094-4105.
57. Muller P, Rossler J, Schwarz-Finsterle J, Schmitt E, Hausmann M. PNA-COMBO-FISH: From combinatorial probe design in silico to vitality compatible, specific labelling of gene targets in cell nuclei. Exp Cell Res. 2016; 345: 51-59.
58. Schmitt E, Schwarz-Finsterle J, Stein S, Boxler C, Muller P, Mokhir A, et al. COMBinatorial Oligo FISH: directed labeling of specific genome domains in differentially fixed cell material and live cells. Methods Mol Biol. 2010; 659: 185-202.
59. Kepper N, Schmitt E, Lesnussa M, Weiland Y, Eussen HB, Grosveld FG, et al. Visualization, analysis, and design of COMBO-FISH probes in the grid-based GLOBE 3D genome platform. Stud Health Technol Inform. 2010; 159: 171-180.

60. Geer LY, Marchler-Bauer A, Geer RC, Han L, He J, He S, et al. The NCBI BioSystems database. Nucleic Acids Res. 2010; 38: D492-496.
61. Zeller D, Kepper N, Hausmann M, Schmitt E, editors. Sequential and structural biophysical aspects of combinatorial oligo FISH in Her2/neu breast cancer diagnostics. International Symposium on Biomedical Engineering and Medical Physics, 10-12 October, 2012, Riga, Latvia; 2013 2013//; Berlin, Heidelberg: Springer Berlin Heidelberg.
62. Schwarz-Finsterle J, Stein S, Grossmann C, Schmitt E, Trakhtenbrot L, Rechavi G, et al. Comparison of triple helical COMBO-FISH and standard FISH by means of quantitative microscopic image analysis of abl/bcr positions in cell nuclei. J Biochem Biophys Methods. 2007; 70: 397-406.
63. Schwarz-Finsterle J, Stein S, Grossmann C, Schmitt E, Schneider H, Trakhtenbrot L, et al. COMBO-FISH for focussed fluorescence labelling of gene domains: 3D-analysis of the genome architecture of abl and bcr in human blood cells. Cell Biol Int. 2005; 29: 1038-1046.
64. Grossmann C, Schwarz-Finsterle J, Schmitt E, Birk U, Hildenbrand G, Cremer C, et al. Variations of the spatial fluorescence distribution in ABL gene chromatin domains measured in blood cell nuclei by SMI microscopy after COMBO – FISH labelling2010.
65. Krufczik M, Sievers A, Hausmann A, Lee JH, Hildenbrand G, Schaufler W, et al. Combining low temperature fluorescence DNA-hybridization, immunostaining, and super-resolution localization microscopy for nano-structure analysis of ALU elements and their influence on chromatin structure. Int J Mol Sci. 2017; 18.
66. Lemmer P, Gunkel M, Weiland Y, Muller P, Baddeley D, Kaufmann R, et al. Using conventional fluorescent markers for far-field fluorescence localization nanoscopy allows resolution in the 10-nm range. J Microsc. 2009; 235: 163-171.
67. Cremer C, Kaufmann R, Gunkel M, Pres S, Weiland Y, Muller P, et al. Superresolution imaging of biological nanostructures by spectral precision distance microscopy. Biotechnol J. 2011; 6: 1037-1051.
68. Huang B, Bates M, Zhuang X. Super-resolution fluorescence microscopy. Annu Rev Biochem. 2009; 78: 993-1016.
69. Baddeley D, Crossman D, Rossberger S, Cheyne JE, Montgomery JM, Jayasinghe ID, et al. 4D super-resolution microscopy with conventional fluorophores and single wavelength excitation in optically thick cells and tissues. PLoS One. 2011; 6: e20645.
70. Alinezhad S, Vaananen RM, Ochoa NT, Vertosick EA, Bjartell A, Bostrom PJ, et al. Global expression of AMACR transcripts predicts risk for prostate cancer - a systematic comparison of AMACR protein and mRNA expression in cancerous and noncancerous prostate. BMC Urol. 2016; 16: 10.
71. Ferdinandusse S, Denis S, L IJ, Dacremont G, Waterham HR, Wanders RJ. Subcellular localization and physiological role of alpha-methylacyl-CoA racemase. J Lipid Res. 2000; 41: 1890-1896.
72. Luo J, Zha S, Gage WR, Dunn TA, Hicks JL, Bennett CJ, et al. Alpha-methylacyl-CoA racemase: a new molecular marker for prostate cancer. Cancer Res. 2002; 62: 2220-2226.
73. Rubin MA, Zhou M, Dhanasekaran SM, Varambally S, Barrette TR, Sanda MG, et al. alpha-Methylacyl coenzyme A racemase as a tissue biomarker for prostate cancer. JAMA. 2002; 287: 1662-1670.

74. Zha S, Isaacs WB. A nonclassic CCAAT enhancer element binding protein binding site contributes to alpha-methylacyl-CoA racemase expression in prostate cancer. Mol Cancer Res. 2005; 3: 110-118.
75. Jiang N, Zhu S, Chen J, Niu Y, Zhou L. A-methylacyl-CoA racemase (AMACR) and prostate-cancer risk: A meta-analysis of 4,385 participants. Plos One. 2013; 8: e74386.
76. Wiech T, Stein S, Lachenmaier V, Schmitt E, Schwarz-Finsterle J, Wiech E, et al. Spatial allelic imbalance of BCL2 genes and chromosome 18 territories in nonneoplastic and neoplastic cervical squamous epithelium. Eur Biophys J. 2009; 38: 793-806.
77. Boyd PS, Struve N, Bach M, Eberle JP, Gote M, Schock F, et al. Clustered localization of EGFRvIII in glioblastoma cells as detected by high precision localization microscopy. Nanoscale. 2016; 8: 20037-20047.
78. Pilarczyk G, Nesnidal I, Gunkel M, Bach M, Bestvater F, Hausmann M. Localisation microscopy of breast epithelial ErbB-2 Receptors and gap junctions: Trafficking after gamma-irradiation, neuregulin-1beta, and trastuzumab application. Int J Mol Sci. 2017; 18.
79. Tanabe H, Habermann FA, Solovei I, Cremer M, Cremer T. Non-random radial arrangements of interphase chromosome territories: evolutionary considerations and functional implications. Mutat Res. 2002; 504: 37-45.
80. Zhang Y, Heermann DW. DNA double-strand breaks: linking gene expression to chromosome morphology and mobility. Chromosoma. 2014; 123: 103-115.
81. Boyle S, Gilchrist S, Bridger JM, Mahy NL, Ellis JA, Bickmore WA. The spatial organization of human chromosomes within the nuclei of normal and emerin-mutant cells. Human Molecular Genetics. 2001; 10: 211-219.
82. Heride C, Ricoul M, Kieu K, von Hase J, Guillemot V, Cremer C, et al. Distance between homologous chromosomes results from chromosome positioning constraints. J Cell Sci. 2010; 123: 4063-4075.
83. Sievers A, Bosiek K, Bisch M, Dreessen C, Riedel J, Fross P, et al. K-mer content, correlation, and position analysis of genome DNA sequences for the identification of function and evolutionary features. Genes (Basel). 2017; 8.
84. Lopez-Flores I, Garrido-Ramos MA. The repetitive DNA content of eukaryotic genomes. Genome Dyn. 2012; 7: 1-28.
85. Plohl M, Luchetti A, Mestrovic N, Mantovani B. Satellite DNAs between selfishness and functionality: structure, genomics and evolution of tandem repeats in centromeric (hetero)chromatin. Gene. 2008; 409: 72-82.
86. Biscotti MA, Olmo E, Heslop-Harrison JS. Repetitive DNA in eukaryotic genomes. Chromosome Res. 2015; 23: 415-420.
87. Deininger P. Alu elements: know the SINEs. Genome Biol. 2011; 12: 236.
88. Batzer MA, Deininger PL. Alu repeats and human genomic diversity. Nat Rev Genet. 2002; 3: 370-379.
89. Han JS, Boeke JD. LINE-1 retrotransposons: modulators of quantity and quality of mammalian gene expression? Bioessays. 2005; 27: 775-784.
90. Prades C, Laurent AM, Puechberty J, Yurov Y, Roizes G. SINE and LINE within human centromeres. J Mol Evol. 1996; 42: 37-43.

91. Birchler JA, Presting GG. Retrotransposon insertion targeting: a mechanism for homogenization of centromere sequences on nonhomologous chromosomes. Gene Dev. 2012; 26: 638-640.
92. Wong LH, Choo KHA. Evolutionary dynamics of transposable elements at the centromere. Trends in Genetics. 2004; 20: 611-616.
93. Schueler MG, Sullivan BA. Structural and functional dynamics of human centromeric chromatin. Annu Rev Genomics Hum Genet. 2006; 7: 301-313.
94. Wang JR, Geesman GJ, Hostikka SL, Atallah M, Blackwell B, Lee E, et al. Inhibition of activated pericentromeric SINE/Alu repeat transcription in senescent human adult stem cells reinstates self-renewal. Cell Cycle. 2011; 10: 3016-3030.
95. Klein SJ, O'Neill RJ. Transposable elements: genome innovation, chromosome diversity, and centromere conflict. Chromosome Res. 2018; 26: 5-23.
96. Mestrovic N, Mravinac B, Pavlek M, Vojvoda-Zeljko T, Satovic E, Plohl M. Structural and functional liaisons between transposable elements and satellite DNAs. Chromosome Res. 2015; 23: 583-596.